# A novel combined fluid dynamic and strain analysis approach identified abdominal aortic aneurysm rupture

Arianna Forneris, PhD,[a] Flavio Bellacosa Marotti, MSc,[a] Alessandro Satriano, PhD,[a] Randy D. Moore, MD,[b] *and* Elena S. Di Martino, PhD,[c] *Calgary, Alberta, Canada*

## ABSTRACT

Clinical decision-making for surgical repair of abdominal aortic aneurysms based on maximum aortic diameter presents limitations as rupture can occur below threshold for some aneurysms, whereas others are stable at large sizes. The proposed approach combines hemodynamics and geometric indices with in vivo deformation analysis to assess local weakening of the aortic wall for a case of impending rupture that was confirmed during open surgical repair. A new combined index, the Regional Rupture Potential, is introduced to help the assessment of individual aneurysms and their rupture risk, providing a rationale for clinical decisions. (J Vasc Surg Cases and Innovative Techniques 2020;6:172-6.)

**Keywords:** Abdominal aortic aneurysm (AAA); Computational fluid dynamics (CFD); Thrombosis (ILT); In vivo strain; Rupture

Clinical management of abdominal aortic aneurysm (AAA) currently relies on assessment of the maximum aortic diameter as a marker of rupture risk. A significant individual variability has been reported, however, highlighting the limits of the AAA maximum diameter as a sole index of rupture risk.[1,2]

Local hemodynamic forces are known to have a crucial role in regulating vascular function as well as in promoting local structural remodeling in response to long-term flow alterations.[3-6] Aortic expansion and rupture have been associated with regions of low wall shear stress load (<0.4 Pa) and intraluminal thrombus (ILT) accumulation.[7-10] Local wall deformability relates to local mechanical properties and aortic function[11,12]; however, a clear indicator pointing to a localized weakening of the aortic wall has yet to be found.

This study proposes to assess the deformation of the AAA wall through in vivo strain measurements and to combine the resulting strain map with local ILT thickness and hemodynamic indices obtained by means of computational fluid dynamics (CFD). The resulting combined index, Regional Rupture Potential (RRP; U.S. Patent and Trademark Office 62/906,980), may help the assessment of individual aortas, providing a rationale for clinical decisions and rupture risk stratification.

The study protocol was approved by the University of Calgary Conjoint Health Research Ethics Board. The patient's informed consent and permission for publication was obtained before study enrollment and data collection.

## CASE REPORT

A 62-year-old man with infrarenal AAA (diameter, 5.6 cm; smoking history, no hypertension or comorbidities) was admitted to the hospital and consented to participate in a Conjoint Health Research Ethics Board-approved protocol that includes preoperative electrocardiography-gated dynamic computed tomography (CT) imaging.

Shortly before imaging, the patient developed sudden severe abdominal and back pain. CT scan showed early signs of impending rupture,[13] including periaortic fat stranding as reported by the radiologist (Fig 1). Aortic geometry and hemodynamics were preserved at the time of imaging; the patient presented with an unusual case of rupture in evolution, providing a unique timeline for our analysis. Open aortic tube graft repair was performed on the patient, and CT images were transferred to the research analysis team without their knowledge of the clinical events, nor was the research team made aware of the location of the rupture until after the analysis had been completed.

The commercial imaging software Simpleware ScanIP (Synopsys, Mountain View, Calif) was used for image processing and segmentation of aortic lumen and wall. The two geometries were then imported in ICEM (ANSYS, Canonsburg, Pa) for discretization. ILT thickness was obtained as normal distance between the AAA outer wall and lumen surfaces using a custom MATLAB (MathWorks, Natick, Mass) routine.

From the Biomedical Engineering Graduate Program,[a] Department of Surgery,[b] and Civil Engineering, Centre for Bioengineering Research and Education, Libin Cardiovascular Institute of Alberta,[c] University of Calgary.

This work was supported by the Werner Graupe International Fellowship in Engineering, with contributions from the National Science and Engineering Research Council of Canada Discovery Grant RGPIN/04043-2014 and the Heart and Stroke Foundation Grant in Aid G 170019141 to E.S.D.M.

Author conflict of interest: E.S.D.M. and R.D.M. are cofounders of the startup company ViTAA. A.F., F.B.M., and A.S. are minor shareholders of ViTAA.

Correspondence: Arianna Forneris, PhD, Calgary Centre for Innovative Technology, University of Calgary, 50 Collegiate Place NW, Calgary, AB T2N 4V8, Canada (e-mail: arianna.forneris@ucalgary.ca).

The editors and reviewers of this article have no relevant financial relationships to disclose per the Journal policy that requires reviewers to decline review of any manuscript for which they may have a conflict of interest.

2468-4287



https://doi.org/10.1016/j.jvscit.2020.01.014

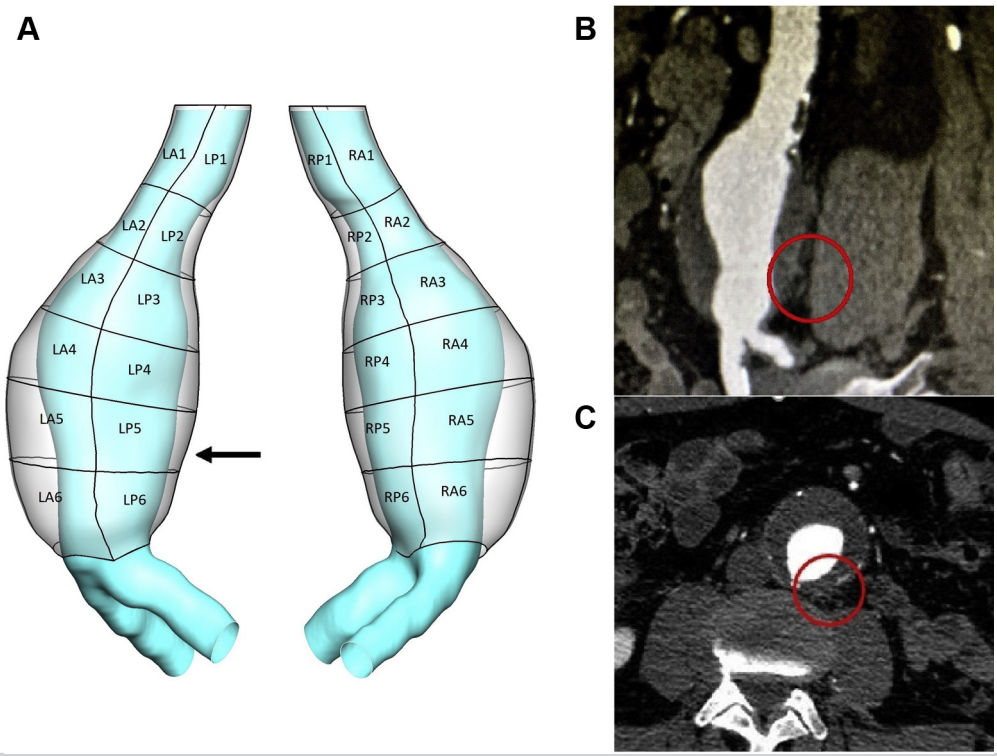


**Fig 1. A,** Three-dimensional geometry (outer wall and lumen) of the abdominal aortic aneurysm (AAA) under investigation. A patching system helped define 24 patches based on location (left, right, anterior, or posterior) and was employed to analyze region-averaged descriptors. The *arrow* indicates the site of rupture at the level of patch LP5. **B,** Left sagittal oblique view of cardiac gated computed tomography (CT) scan demonstrating periaortic fat stranding as early sign of contained rupture at the left posterolateral portion of aortic wall (*circle*). **C,** Axial view of cardiac gated CT scan showing location of rupture in evolution at around 5 o'clock on the clock face (*circle*).

**CFD analysis.** A volumetric mesh of approximately 4 million tetrahedral elements was selected after sensitivity analysis and used to run CFD simulations in FLUENT (ANSYS), employing a SIMPLE algorithm and a second-order implicit transient formulation. Blood flow was assumed to be laminar, and a time-varying velocity profile based on flow rate in the descending aorta was prescribed at the inlet of the fluid domain, as reported by Mills at al.[14] An outflow boundary condition was imposed with 50% flow division to the iliac arteries.

The rheologic model assumed the blood to be an isotropic, incompressible, Newtonian fluid[15] with assigned constant density (1060 kg/m$^3$) and dynamic viscosity (0.00319 Pa·s). The arterial wall was assumed to be rigid, and no-slip conditions were applied at the fluid interface. Time-averaged wall shear stress (TAWSS) was derived from CFD results to quantify local hemodynamic disturbances as described in previous publications.[3]

**Strain analysis.** Three-dimensional principal strain analysis from dynamic CT images (0.7- × 0.7- × 2.0-mm spatial resolution, 0.35-second gantry rotation time) was performed using proprietary MATLAB-based software ViTAA (Virtual Touch Aortic Aneurysm; patent WO-2018/068153-A1) to assess the aneurysm wall strength and weakening index. A surface wall mesh (approximately 4000 triangular shell elements) was used to track node velocities on three-dimensional image stacks representing the aorta through the cardiac cycle. From the velocities, the nodal displacements were measured and used to compute in vivo strain, as presented and validated in previous publications.[11,16] The method ensures in vivo strain computation directly from node displacements so that no constitutive model assumptions are needed (unlike in a finite element simulation).

**Patching and statistical analysis.** Twenty-four patches were defined on the geometries (outer wall and lumen) by sectioning the vessel perpendicular to the lumen centerline (Fig 1), enabling statistical analysis on region-averaged descriptors. A categorization method based on quartiles was applied on the averaged variables of interest to assign a category to each patch and to ease the interpretation of the results. The following quartiles were used to define each category range for this case:

category score 1 for region-averaged TAWSS, 0 to 0.464 Pa; ILT, 0 to 2.858 mm; and strain, 0 to 0.024;

category score 2 for region-averaged TAWSS, 0.465 to 0.586 Pa; ILT, 2.859 to 5.076 mm; and strain 0.025 to 0.026;

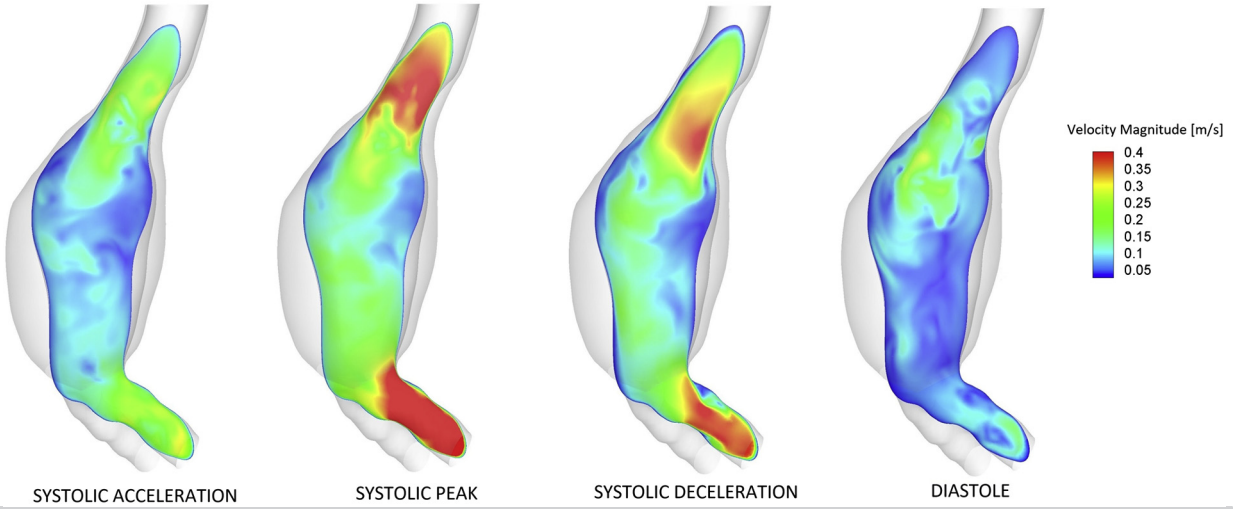


**Fig 2.** Computational fluid dynamics (CFD)-predicted velocity contours on a longitudinal cross section of the abdominal aortic aneurysm (AAA) at different times of the cardiac cycle. *From left*: Systolic acceleration, systolic peak, systolic deceleration, diastole. It is possible to appreciate the presence of a main flow channel originating in the neck and characterized by higher velocities. Lower velocities and recirculation are present in the aneurysmal sac, especially at the level of the rupture site. The shade of both lumen and wall geometry is shown.

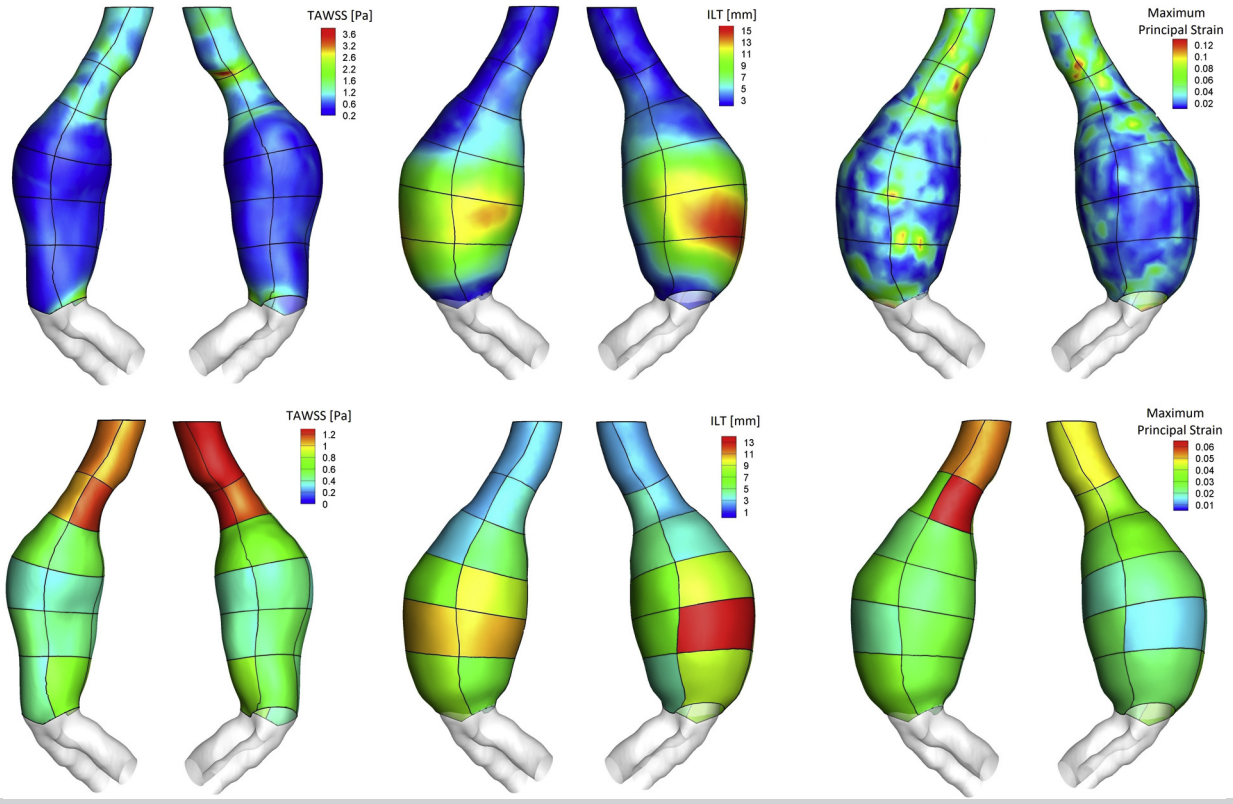


**Fig 3.** *Top*, Distribution of time-averaged wall shear stress (*TAWSS*) on luminal surface, intraluminal thrombus (*ILT*) thickness on wall surface, and maximum principal strain on wall surface. The outline of the patches is visible on top of the distribution. *Bottom*, Distribution of region-averaged TAWSS on luminal surface, region-averaged ILT thickness on wall surface, and region-averaged maximum principal strain on wall surface.

category score 3 for region-averaged TAWSS, 0.587 to 1.120 Pa; ILT, 5.077 to 8.287 mm; and strain 0.027 to 0.038; and category score 4 for region-averaged TAWSS, 1.121 to 1.294 Pa; ILT, 8.288 to 13.133 mm; and strain 0.039 to 0.060.

The RRP was obtained as the sum of the category scores on each single patch and then converted to a percentage value. Regional correlations were analyzed by means of Spearman coefficient (statistical significance at $P < .05$).

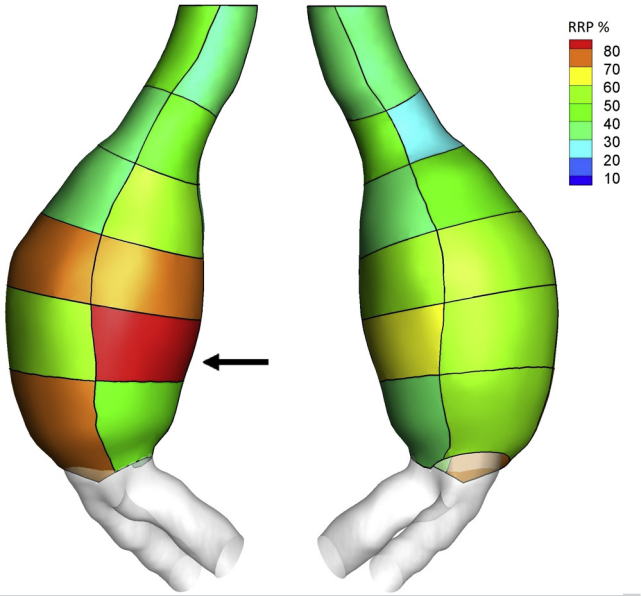


**Fig 4.** Regional Rupture Potential (*RRP*) index computed on patches on the aortic wall surface. The *arrow* indicates the site of rupture at the level of patch LP5.

## RESULTS

The flow pattern in the lumen was characterized by recirculation and low velocities at the aneurysmal sac where low TAWSS and thick ILT predominated (Figs 2 and 3). A strong negative correlation was found between region-averaged TAWSS and ILT thickness ($\rho = -0.78$; $P = 5.9e\text{-}06$).

A main flow channel associated with high velocity was visible in the neck and in areas of flow impingement onto the aortic wall, where it resulted in high TAWSS, almost no ILT, and high strain (Figs 2 and 3), pointing to a moderate correlation between region-averaged TAWSS and maximum principal strain ($\rho = 0.60$; $P = .002$) and between region-averaged ILT and strain ($\rho = -0.61$; $P = .001$).

Intraoperatively, the aortic wall demonstrated periaortic edema at the 5-o'clock position along the left posterolateral wall, at the level of patch LP5, as well as a small intramural hematoma consistent with the impending rupture noted on the preoperative CT scan; no free blood was present in the peritoneal cavity. After opening of the aortic sac, an obvious rent through the aortic wall was identified, corresponding to the area in question, which does not correspond to the location of maximum diameter. This region presented with low TAWSS, thick ILT, and high maximum principal strain, corresponding to an RRP indicating a weak wall (Fig 4). The Table shows all patch-averaged values and the corresponding category score for each descriptor. Patch LP5 was assigned category score 1 for TAWSS (low TAWSS, converted to score 4 in the RRP calculation to assign a higher risk to low TAWSS regions according to the observations that low TAWSS correlates with ILT deposition, enlargement, and wall rupture[8,9]), category score 4 for ILT (thick thrombus), and category score 3 for strain (high deformability).

**Table.** Summary of patch-averaged values for the time-averaged wall shear stress (*TAWSS*), intraluminal thrombus (*ILT*), and maximum principal strain and the category scores assigned to each patch for each variable of interest through a quartile-based categorization method

| Patch | TAWSS, Pa, patch averaged | TAWSS score | ILT, mm, patch averaged | ILT score | Strain patch averaged | Strain score |
|---|---|---|---|---|---|---|
| LA1 | 1.119 | 3 | 2.573 | 1 | 0.052 | 4 |
| LP1 | 1.121 | 4 | 2.723 | 1 | 0.056 | 4 |
| RP1 | 1.279 | 4 | 2.559 | 1 | 0.046 | 4 |
| RA1 | 1.294 | 4 | 2.442 | 1 | 0.049 | 4 |
| LA2 | 1.046 | 3 | 2.533 | 1 | 0.029 | 3 |
| LP2 | 1.202 | 4 | 3.735 | 2 | 0.060 | 4 |
| RP2 | 1.206 | 4 | 4.062 | 2 | 0.039 | 4 |
| RA2 | 1.121 | 4 | 2.716 | 1 | 0.035 | 3 |
| LA3 | 0.559 | 2 | 2.994 | 2 | 0.024 | 1 |
| LP3 | 0.519 | 2 | 5.391 | 3 | 0.025 | 2 |
| RP3 | 0.606 | 3 | 4.760 | 2 | 0.025 | 2 |
| RA3 | 0.623 | 3 | 3.795 | 2 | 0.032 | 3 |
| LA4 | 0.377 | 1 | 6.994 | 3 | 0.027 | 3 |
| LP4 | 0.398 | 1 | 9.146 | 4 | 0.026 | 2 |
| RP4 | 0.401 | 1 | 6.902 | 3 | 0.018 | 1 |
| RA4 | 0.465 | 2 | 8.895 | 4 | 0.023 | 1 |
| LA5 | 0.506 | 2 | 10.681 | 4 | 0.020 | 1 |
| LP5 | 0.463 | 1 | 10.741 | 4 | 0.031 | 3 |
| RP5 | 0.428 | 1 | 6.236 | 3 | 0.026 | 2 |
| RA5 | 0.522 | 2 | 13.133 | 4 | 0.014 | 1 |
| LA6 | 0.444 | 1 | 7.986 | 3 | 0.037 | 3 |
| LP6 | 0.703 | 3 | 5.760 | 3 | 0.025 | 2 |
| RP6 | 0.791 | 3 | 3.958 | 2 | 0.025 | 2 |
| RA6 | 0.566 | 2 | 8.589 | 4 | 0.024 | 1 |

Row LP5 corresponds to the region of rupture.

## DISCUSSION

Aneurysm rupture occurred at a site of reduced blood flow velocity, characterized by recirculation and associated with low TAWSS and thick thrombus deposition in agreement with previously reported findings.[7-9] Although the shear stress is unlikely to be the direct cause of rupture, the strong correlation between patch-averaged TAWSS and ILT suggests a mechanism of thrombus deposition at locations of disturbed flow where low oscillatory wall shear stress predominates. The effect of ILT accumulation may contribute to local

inflammatory processes and hypoxia, leading to adverse remodeling and loss of structural integrity indicating disease progression.[17-19]

The heterogeneous remodeling is reflected in the local in vivo deformation. A moderate regional correlation between TAWSS and strain was found as a possible consequence of main flow channel impingement (neck, LA3, RA3, LA6). The ruptured patch, however, exhibited an opposite trend, showing low TAWSS and high maximum principal strain, resulting in a high RRP index as an indication of localized weakening (Figs 3 and 4). Comparison of RRP throughout the aneurysm wall highlighted the area corresponding to the impending rupture as the area at the highest risk of rupture locally for this aneurysm.

Despite being common to most AAAs, thrombus formation is not present in all aneurysms; the absence of ILT does not compromise the RRP calculation aimed at identifying areas of large strain and low TAWSS, where wall deformability is likely to be a consequence of local weakening. Although at this stage the index was able to predict the rupture location rather than occurrence, the presented approach provides insight on wall regional weakening that could improve aortic assessment for risk stratification purposes.

## CONCLUSIONS

This study was limited to one ruptured patient and assumed a rigid aortic wall for CFD simulations. The assumption of rigid wall is considered acceptable and accurate in capturing the main flow features in the context of unknown wall and thrombus material properties and increased computational cost introduced by a simulation with moving walls.[20] Despite the limitations, our results point to the importance of local descriptors in assessing aortic wall vulnerability and suggest that combined fluid dynamics and strain analysis may assist in estimating the rupture potential of individual aneurysms.

The authors wish to acknowledge Mr Richard Beddoes for help with strain analysis.

## REFERENCES

1. Geroulakos G, Nicolaides A. Infrarenal abdominal aortic aneurysms less than five centimeters in diameter: the surgeon's dilemma. Eur J Vasc Surg 1992;6:622-61.
2. Choksy SA, Wilmink AB, Quick CR. Ruptured abdominal aortic aneurysm in the Huntingdon district: a 10-year experience. Ann R Coll Surg Engl 1999;81:27-31.
3. Martufi G, Forneris A, Nobakht S, Rinker KD, Moore RD, Di Martino ES. Case study: intra-patient heterogeneity of aneurysmal tissue properties. Front Cardiovasc Med 2018;5:82.
4. Chien S. Mechanotransduction and endothelial cell homeostasis: the wisdom of the cell. Am J Physiol Heart Circ Physiol 2007;292:H1209-24.
5. Chiu JJ, Chien S. Effects of disturbed flow on vascular endothelium: pathophysiological basis and clinical perspectives. Physiol Rev 2011;91:327-87.
6. Bonert M, Leask RL, Butany J, Ethier CR, Myers JG, Johnston KW, et al. The relationship between wall shear stress distributions and intimal thickening in the human abdominal aorta. Biomed Eng Online 2003;2:18.
7. Doyle BJ, McGloughlin TM, Kavanagh EG, Hoskins PR. From detection to rupture: a serial computational fluid dynamics case study of a rapidly expanding, patient-specific, ruptured abdominal aortic aneurysm. In: Doyle B, Miller K, Wittek A, Nielsen P, editors. Computational biomechanics for medicine. New York: Springer; 2014. p. 53-68.
8. Boyd AJ, Kuhn DCS, Lozowy RJ, Kulbisky GP. Low wall shear stress predominates at sites of abdominal aortic aneurysm rupture. J Vasc Surg 2015;63:1613-9.
9. Zambrano BA, Gharahi H, Lim C, Jaberi FA, Choi J, Lee W, et al. Association of intraluminal thrombus, hemodynamic forces, and abdominal aortic aneurysm expansion using longitudinal CT images. Ann Biomed Eng 2015;44:1502-14.
10. Stevens RR, Grytsan A, Biasetti J, Roy J, Lindquist Liljeqvist M, Gasser TC. Biomechanical changes during abdominal aortic aneurysm growth. PLoS One 2017;12:e0187421.
11. Satriano A, Rivolo S, Martufi G, Finol EA, Di Martino ES. In vivo strain assessment of the abdominal aortic aneurysm. J Biomech 2015;48:354-60.
12. Di Martino ES, Guadagni G, Fumero A, Ballerini G, Spirito R, Biglioli P, et al. Fluid-structure interaction within realistic three-dimensional models of the aneurysmatic aorta as a guidance to assess the risk of rupture of the aneurysm. Med Eng Phys 2001;23:647-55.
13. Gish DS, Baer JA, Crabtree GS, Shaikh B, Fareedy SB. Impending aortic aneurysm rupture—a case report and review of the warning signs. J Community Hosp Intern Med Perspect 2016;6:32217.
14. Mills C, Gabe I, Gault J, Mason D, Ross JJ, Brunwald E, et al. Pressure-flow relationships and vascular impedance in man. Cardiovasc Res 1970;4:405-17.
15. Berger SA, Jou LD. Flows in stenotic vessels. Annu Rev Fluid Mech 2000;32:347-82.
16. Satriano A, Guenther Z, White JA, Merchant N, Di Martino ES, Al-Qoofi F, et al. Three-dimensional thoracic aorta principal strain analysis from routine ECG-gated computerized tomography: feasibility in patients undergoing transcatheter aortic valve replacement. BMC Cardiovasc Disord 2018;18:76.
17. Vorp DA, Lee PC, Wang DH, Makaroun MS, Nemoto EM, Ogawa S, et al. Association of intraluminal thrombus in abdominal aortic aneurysm with local hypoxia and wall weakening. J Vasc Surg 2001;34:291-9.
18. Wilson JS, Virag L, Di Achille P, Karsaj I, Humphrey JD. Biochemomechanics of intraluminal thrombus in abdominal aortic aneurysms. J Biomech Eng 2013;135:021011.
19. Martufi G, Satriano A, Moore RD, Vorp DA, Di Martino ES. Local quantification of wall thickness and intraluminal thrombus offer insight into the mechanical properties of the aneurysmal aorta. Ann Biomed Eng 2015;43:1759-71.
20. Brown AG, Shi Y, Marzo A, Staicu C, Valverde I, Beerbaum P, et al. Accuracy vs. computational time: translating aortic simulations to the clinic. J Biomech 2012;45:516-23.

Submitted Apr 16, 2019; accepted Jan 25, 2020.